Computer Assisted Mechanics and Engineering Sciences, 7: 207–218, 2000.

Numerical solution of the thermomechanical processes in the thin layer structure of thermal barrier[1]

Josef Kuneš and Zdeněk Veselý[2]
West Bohemia University, Faculty of Applied Sciences, Department of Physics
Univerzitní 22, Plzeň, 306 14, Czech Republic

(Received March 8, 1999)

High demands for dynamic thermal insulating protection of machine parts lead to the development of thermal barriers. The mathematical and simulation model has been developed to simulate thermomechanical processes during thermal shock on the surface of different thermal barrier structures. The finite element method has been applied to the heterogeneous thin layer structure of the thermal barrier. Temperature, temperature gradient, heat flux, thermally induced stress and strain have been chosen as the characteristics describing the dynamic behaviour of the thermal barrier during the thermal shock. Results of the simulation for several alternatives of thermal barrier are discussed to summarize the effect of characteristic parameters of the thermal barrier to its dynamic behaviour.

Keywords: computer simulation, FEM, thermomechanical processes, thermal barrier, special industrial application

1. Introduction

Thermal barriers (TB) protect the material of machine parts against high temperatures and thermal shocks. Their importance increases with the orientation to more powerful and economical energy appliances and further in recent advanced manufacturing technologies. TB's usually represent a heterogeneous multilayer coating deposited on the surface of the thermal loaded machine part those temperature should be decreased. Potential advantages of thermal barriers can be summarized into following:

- Keeping the substrate surface temperature of TB-protected machine part at the same value, the appliance operation temperature can be increased along with the increase of the TB thickness that means the higher appliance efficiency.
- On the other hand, using the TB-protected machine part along with keeping the appliance operation temperature at the same value, it leads to the decrease of substrate surface temperature that means the increase of machine part operation lifetime.

The objective of this paper is to shortly point out some specific problems arising from the numerical solution of thermomechanical processes in the TB-substrate system especially during a thermal shock and to show the dynamic behaviour of basic structures of TB in the TB-substrate system. From the physical point of view, it concerns the problem of a non-stationary nonlinear heat and stress distributions in the structured system involving several thin layers of TB and the relatively thick substrate. TB's usually consist of the top ceramic layer, the additional layer and the bond coat. Thermal and mechanical properties of these layers are essentially different. It considerably affects the dynamics of thermal and especially thermal induced stress processes.

[1]Abbreviated version of this paper was presented at the VII Conference *Numerical Methods in Continuum Mechanics*, Stará Lesná, High Tatras, Slovakia, October 6–9, 1998, and published in its Proceedings.

[2]corresponding author

2. Physical structure of thermal barriers

The TB structure is given by the technological and operational requirements. The top ceramic layer, usually ZrO_2, must have high thermal resistivity, sufficient reflectance for infra-red radiation and must satisfy stress and strain conditions. The thickness of the ceramic layer usually ranges from 100 to 500 μm. The bond coat must offer fair tolerance against high temperature corrosion and oxidation. Further, the bond coat helps binding the ceramic layer to the substrate and helps accommodating the mechanical deformation caused by different coefficients of thermal expansion and modulus of elasticity for the ceramic layer and the substrate. The bond coat thickness ranges from 100 to 300 μm. The additional layer, made of Al_2O_3, has usually the thickness roughly from 1 to 5 μm. This layer represents the diffusion barrier that decreases an oxidation of the bond coat and the underlaying substrate.

The thermal conductivity of the ceramic layer is usually about one order lower than of the substrate representing high thermal resistance on the surface. The high thermal resistance decreases the effect of high temperatures and temperature shocks on the surface. The effects of thickness, porosity and thermomechanical properties of each layer to the dynamic behaviour of the TB are the important questions to be solved during the design of TB's. The dynamic behaviour is characterized by the temperature, temperature gradient, heat flux, thermally induced stress and strain, especially at the interface between the individual layers.

The detailed information about the TB physical structure, production, test performance, lifetime modelling, etc., can be found in a relatively numerous literature, particularly in [1, 3, 4, 7, 11, 14, 15, 16, 18].

3. Mathematical model

The machine parts of high temperature appliances are subjected during the operation conditions to various modes of damage including the difference between the thermal expansion coefficients of the ceramic layer and the substrate, phase transformations within the ZrO_2, erosion, oxidation and high temperature corrosion by molten salts. TB's should be tolerant to these failure modes and should stay well bonded to the substrate during the requested lifetime.

It is impossible to include all of these complicated processes to the computer simulation. The reaction of the TB-substrate structure only at the beginning short time period after the thermal shock on the TB surface is investigated here. Therefore, the processes that are important during long term cyclic thermal loading such as phase transformation within ZrO_2, oxidation, high temperature corrosion by molten salts, etc. are not taken into account. Only the thermomechanical process of heat transfer and thermally induced stress and strain with the consideration of the elastic mechanical properties is simulated within the TB-substrate structure.

Thermomechanical process in the structure of the TB represents a conjugate process comprising heat transfer and thermally induced stress and strain. Perfect contact between individual layers of a TB and substrate is supposed.

Non-stationary nonlinear heat conduction in individual layers of the TB and the substrate is given by the equation

$$\frac{\partial T}{\partial t} = \frac{1}{C(T)} \frac{\partial}{\partial x_i} \left(\lambda(T) \frac{\partial T}{\partial x_i} \right) + \frac{q_v}{C(T)} \tag{1}$$

where $C(T) = c(T)\rho(T)$, $c(T)$, $\rho(T)$, $\lambda(T)$, q_v, T, t and x_i are temperature dependent volume thermal capacity [J·m^{-3}·K^{-1}], temperature dependent specific thermal capacity [J·kg^{-1}·K^{-1}], temperature dependent density, temperature dependent coefficient of thermal conductivity, inner heat source, temperature, time and space variables, respectively.

Temperature distribution in the TB induces thermal stress and strain. In the case of a three dimensional thermally induced stress, six relations between stresses and strains, six relations between

displacements and strains and three equations of continuum equilibrium are to be solved. Fifteen unknown quantities are determined from these relations. These quantities contain six components of the stress tensor σ_{ij}, six components of the strain tensor e_{ij} and three components of the displacement vector u_i. The thermally induced stress problem is much more easier, if some quantities are equal to zero or negligible arising from geometry or loads. In the case of plane stress in the plane vertical to the z axis, the following conditions state

$$\sigma_{zz} = \sigma_{zx} = \sigma_{zy} = 0. \tag{2}$$

The relations between strains, displacements and stresses are then

$$e_{xx} = \frac{\partial u_x}{\partial x} = \frac{1}{E(T)}[\sigma_{xx} - \nu(T)\sigma_{yy}] + \alpha(T)T\,, \tag{3}$$

$$e_{yy} = \frac{\partial u_y}{\partial y} = \frac{1}{E(T)}[\sigma_{yy} - \nu(T)\sigma_{xx}] + \alpha(T)T\,, \tag{4}$$

$$e_{xy} = \frac{\partial u_x}{\partial y} + \frac{\partial u_y}{\partial x} = \frac{1}{G(T)}\sigma_{xy}\,, \tag{5}$$

where $E(T)$ is temperature dependent modulus of elasticity, $\nu(T)$ is temperature dependent Poisson's ratio, $\alpha(T)$ is temperature dependent coefficient of thermal expansion and $G(T)$ is temperature dependent shear modulus

$$G(T) = \frac{E(T)}{2(1+\nu(T))}\,.$$

The equilibrium equations are

$$\frac{\partial \sigma_{xx}}{\partial x} + \frac{\partial \sigma_{yx}}{\partial y} + f_x = 0, \tag{6}$$

$$\frac{\partial \sigma_{xy}}{\partial x} + \frac{\partial \sigma_{yy}}{\partial y} + f_y = 0, \tag{7}$$

where f_i is the volume strength vector.

The above equations (1)–(7) are supplemented with thermal boundary conditions of the first kind (surface temperature), of the second kind (surface heat flux) and with the boundary surface displacement

$$T(s,t) = F(s,t), \qquad Q(s,t) = -\lambda(T)\frac{\partial T(s,t)}{\partial n}\,, \tag{8}$$

$$u_i(s,t) = L_i(s,t), \tag{9}$$

where $F(s,t)$, $Q(s,t)$ and $L_i(s,t)$ are prescribed functions at all surface points s and time t, n is the outer normal to the surface at the point s.

Initial conditions are

$$T(x,t) = V(x), \qquad \sigma_{ij}(x,t) = W_{ij}(x), \tag{10}$$

where $V(x)$ and $W_{ij}(x)$ are prescribed functions at all inner points x.

Equations (1)–(10) represent the differential mathematical model of the temperature and thermally induced stress processes in the TB-substrate system. Detailed information about mathematical description of the temperature and thermally induced stress fields can be found in [5].

The FEM model of the thermal problem can be written in the following matrix form

$$[C]\{\dot{T}\} + [L]\{T\} = \{q\} \tag{11}$$

where $[C]$ is the matrix of thermal capacity, $[L]$ is the matrix of thermal conducitivity, $\{q\}$ is the vector of thermal load and $\{T\}$, $\{\dot{T}\}$ are the vectors of temperature and temperature time derivative.

Solving this equation for temperature, the thermally induced stress problem can proceed. The matrix form is

$$\{e\} = [B]\{u\} \tag{12}$$

$$\{\sigma\} = [D](\{e\} - \{e_0\}) \tag{13}$$

where $\{e_0\}$ represents the vector of thermal strain

$$\{e_0\} = \{\alpha\}T, \tag{14}$$

$\{e\}$, $\{\sigma\}$ and $\{u\}$ are the vectors of strain, stress and nodal displacements. $[B]$ is the strain–displacement matrix, $[D]$ is the elasticity matrix and $\{\alpha\}$ is the vector of linear thermal expansion.

Combining the equilibrium conditions (6), (7) with boundary conditions (8), (9) leads to the matrix equation

$$[K]\{u\} = \{f\} \tag{15}$$

where

$$[K] = [B]^T[D][B], \tag{16}$$

$$\{f\} = [B]^T\{\sigma\}. \tag{17}$$

$[K]$ is the standard stiffness matrix and $\{f\}$ is the vector of nodal forces corresponding to the boundary conditions. Further information about FEM modelling of thermal stress problems can be found in [19].

4. Physical properties of TB materials

The TB-substrate structure represents a nonlinear heterogeneous thermomechanical system. It is important to get the sufficiently accurate thermal and mechanical properties of individual TB and substrate materials. Inaccuracy of these material parameters significantly affects the results of a numerical solution, particularly when the dynamic TB behaviour is analyzed.

Following these arguments the detailed analysis of thermal and mechanical properties have been made. The available published experimental data have been collected and analytical temperature dependence of the individual material properties has been proposed.

Thermal conductivity λ, specific thermal capacity c and density ρ belong to the most important thermal parameters, whereas modulus of elasticity E, thermal expansion α and Poisson's ratio ν are the most important mechanical parameters. The following analytical functions of temperature are valid at least for $T \in \langle 273,\ 1273\,\mathrm{K}\rangle$.

4.1. Material properties of ZrO_2

Zirconia oxide is a ceramic material whose thermal and mechanical properties varies significantly with porosity p [-].

Porosity dependence of thermal conductivity λ [$\mathrm{W{\cdot}m^{-1}{\cdot}K^{-1}}$] is given by

$$\lambda = 3.230 \times 10^{-4}T + 1.782 \qquad p\ \langle 0{-}3\%\rangle$$

$$\lambda = 3.840 \times 10^{-4}T + 1.475 \qquad p\ \langle 3{-}10\%\rangle$$

$$\lambda = 5.040 \times 10^{-4}T + 1.252 \qquad p\ \langle 10{-}16\%\rangle$$

$$\lambda = 2.530 \times 10^{-7}T^2 + 1.086 \times 10^{-5}T + 9.442 \times 10^{-1} \qquad p\ \langle 16{-}20\%\rangle$$

$$\lambda = 2.360 \times 10^{-7}T^2 + 1.014 \times 10^{-5}T + 8.826 \times 10^{-1} \qquad p\ \langle 20{-}24\%\rangle$$

$$\lambda = -1.825 \times 10^{-13}T^4 + 6.361 \times 10^{-10}T^3$$
$$-3.818 \times 10^{-7}T^2 + 7.608 \times 10^{-5}T + 5.637 \times 10^{-1} \qquad p\ \langle 24{-}30\%\rangle$$

Porosity dependence of density ρ [kg·m^{-3}] is given by

$\rho = 5950$	$p\ \langle 0{-}3\% \rangle$	$\rho = 4940$	$p\ \langle 16{-}20\% \rangle$
$\rho = 5645$	$p\ \langle 3{-}10\% \rangle$	$\rho = 4695$	$p\ \langle 20{-}24\% \rangle$
$\rho = 5245$	$p\ \langle 10{-}16\% \rangle$	$\rho = 4395$	$p\ \langle 24{-}30\% \rangle$

Other thermal and mechanical material properties of the material are given as

$$c = 6.110 \times 10^{-2}T + 5.650 \times 10^{2} - 1.141 \times 10^{7}T^{-2} \quad [\mathrm{J{\cdot}kg^{-1}{\cdot}K^{-1}}]$$
$$\alpha = -2.482 \times 10^{-12}T^{2} + 7.568 \times 10^{-9}T + 4.037 \times 10^{-6} \quad [\mathrm{K^{-1}}]$$
$$E = -5.367 \times 10^{7}T + 1.844 \times 10^{11} \quad [\mathrm{Pa}]$$
$$\nu = 0.290 \quad [-]$$

4.2. Material properties of Nimonic 90

This alloy represents bond coat between ceramic layer and substrate. Chemical composition of Nimonic 90 is 58% Ni – 20% Cr – 18% Co – 3% Ti – 1% Al. Temperature dependence of thermal and mechanical properties is given by

$$\lambda = 2.277 \times 10^{-6}T^{2} + 1.472 \times 10^{-2}T + 7.198 \quad [\mathrm{W{\cdot}m^{-1}{\cdot}K^{-1}}]$$
$$c = 2.130 \times 10^{-8}T^{2} + 5.738 \times 10^{-1}T + 8.155 \times 10^{1} \quad [\mathrm{J{\cdot}kg^{-1}{\cdot}K^{-1}}]$$
$$\rho = -1.397 \times 10^{-4}T^{2} - 1.900 \times 10^{-1}T + 8.336 \times 10^{3} \quad [\mathrm{kg{\cdot}m^{-3}}]$$
$$\alpha = 3.734 \times 10^{-12}T^{2} + 4.109 \times 10^{-10}T + 1.124 \times 10^{-5} \quad [\mathrm{K^{-1}}]$$
$$E = -8.103 \times 10^{1}T^{3} + 2.046 \times 10^{4}T^{2} + 1.346 \times 10^{7}T + 2.129 \times 10^{11} \quad [\mathrm{Pa}]$$
$$\nu = 1.509 \times 10^{-8}T^{2} + 1.161 \times 10^{-5}T + 3.136 \times 10^{-1} \quad [-]$$

4.3. Material properties of steel ČSN 17246

Refractory steel ČSN 17246 represents substrate. Chemical composition of this steel is Fe – 17.0–20.0% Cr – 8.0–11.0% Ni – max. 2.0% Mn – max. 1.0% Si – max. 0.12% C – max. 0.045% P – max. 0.030% S. Temperature dependence of thermal and mechanical properties is given by

$$\lambda = 3.959 \times 10^{-6}T^{2} + 9.015 \times 10^{-3}T + 1.292 \times 10^{1} \quad [\mathrm{W{\cdot}m^{-1}{\cdot}K^{-1}}]$$
$$c = -1.144 \times 10^{-4}T^{2} + 3.102 \times 10^{-1}T + 3.934 \times 10^{2} \quad [\mathrm{J{\cdot}kg^{-1}{\cdot}K^{-1}}]$$
$$\rho = -2.505 \times 10^{-5}T^{2} - 0.400T + 8.016 \times 10^{3} \quad [\mathrm{kg{\cdot}m^{-3}}]$$
$$E = 2.331 \times 10^{4}T^{2} - 1.013 \times 10^{8}T + 2.238 \times 10^{11} \quad [\mathrm{Pa}]$$
$$\alpha = -1.204 \times 10^{-12}T^{2} + 5.723 \times 10^{-9}T + 1.457 \times 10^{-5} \quad [\mathrm{K^{-1}}]$$
$$\nu = 5.852 \times 10^{-8}T^{2} - 2.456 \times 10^{-5}T + 2.951 \times 10^{-1} \quad [-]$$

The tabular data for the TB individual layers and the substrate used to create the above relations are taken mainly from [2, 6, 12, 13, 17].

Table 1. Values of material properties at temperature 673 K

material property	unit	ZrO_2	Nimonic 90	ČSN 17246
thermal conductivity λ	[W·m^{-1}·K^{-1}]	1.066	18.14	20.78
specific thermal capacity c	[J·kg^{-1}·K^{-1}]	580.9	467.7	550.3
density ρ	[kg·m^{-3}]	4940	8145	7735
modulus of elasticity E	[GPa]	148.3	206.5	166.2
thermal expansion α	10^6 [K^{-1}]	8.010	13.21	17.90
Poisson's ratio ν	[-]	0.290	0.328	0.305

The values of TB and substrate material properties at temperature 673 K are presented in Table 1 to show the heterogeneous structure of TB and substrate. ZrO_2 of 16–20% porosity is considered there.

5. Results

The computational system MARC implements transformation of the problem to the computational model utilizing the finite element method (FEM). MARC capabilities of solving non-linearities caused by the temperature dependent material properties and boundary conditions are utilized in modelling the dynamic behaviour of TB under the thermal shock. One interested in using MARC can see [8, 9, 10].

The planar geometry and boundary conditions are plotted in Fig. 1. Zero stress and the temperature of 293 K in the whole TB-substrate structure have been taken as the initial conditions. Elements of the discretization grid within the TB layers have the thickness 5 μm for the proper resolution of the solved quantities in the individual layers of TB and especially near the interface between adjacent layers. The thickness of elements in the substrate is linearly increasing with the distance from the surface. The time step is set to 1 ms.

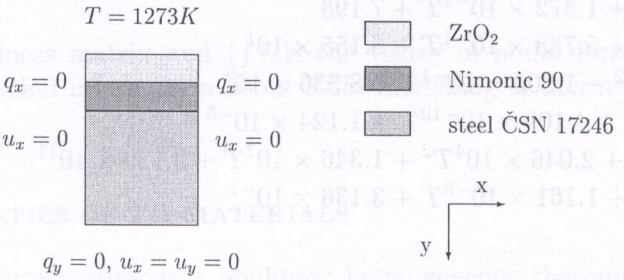

Fig. 1. Geometry and boundary conditions of the model

The effect of the time step on the substrate surface temperature at 1 s for the case of one-layer TB (ZrO_2 of 1 mm thickness and 3–10% porosity) can be seen on the values of the dimensionless temperature $\Theta = T/T_{\text{ref}}$, where T_{ref} is the temperature for the case of time step 1 ms ($\Theta = 1.000$ for the time step 1 ms, $\Theta = 0.999$ for 10 ms, $\Theta = 0.990$ for 100 ms and $\Theta = 0.920$ for 1000 ms).

The effect of the thickness of elements of the discretization grid is similar. The dimensionless temperature is given by $\Theta = T/T_{\text{ref}}$, where T_{ref} is the temperature for the elements thickness 5 μm in the TB ($\Theta = 1.000$ for the elements thickness 5 μm, $\Theta = 0.997$ for 20 μm, $\Theta = 0.989$ for 67 μm and $\Theta = 0.962$ for 250 μm).

A number of the various TB-substrate structures have been solved including raw substrate, one-layer and two-layer TB's.

5.1. Influence of TB parameters on the substrate surface temperature

In the case of the substrate without a TB, surface temperature is 1273 K. With ZrO_2 of 1 mm thickness and 3–10% porosity, substrate surface temperature decreases to 450 K after 1 s. With the increase of the ZrO_2 thickness to 2 mm, substrate surface temperature decreases to 323 K after 1 s. With ZrO_2 of 1 mm thickness and 16–20% porosity, substrate surface temperature decreases only to 383 K after 1 s. By the presence of ZrO_2 of 1 mm thickness and 3–10% porosity and Nimonic 90 of 1 mm thickness, substrate surface temperature decreases to 393 K after 1 s. The greater Nimonic 90 thickness, the lower substrate surface temperature is reached. Considerable influence of the TB on the substrate surface temperature is evident from the above substrate surface temperature values.

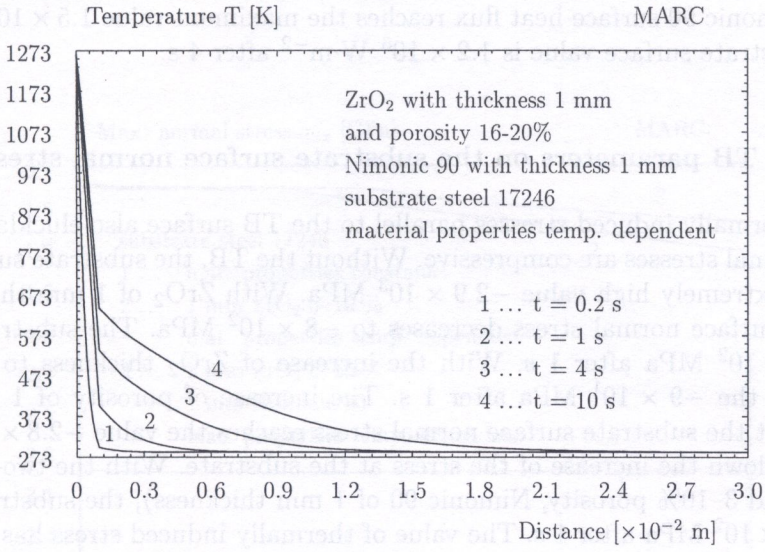

Fig. 2. Temperature dependence on the distance from the surface

The temperature dependence on the distance from the surface at 0.2, 1, 4 and 10 s for the two-layer TB is shown in Fig. 2.

5.2. Influence of TB parameters on the substrate surface temperature gradient

In the case of the substrate without a TB, substrate surface temperature gradient reaches the extremely high value of -4.1×10^5 K·m^{-1} after 0.2 s, -1.8×10^5 K·m^{-1} after 1 s. With ZrO_2 of 1 mm thickness and 3–10% porosity, surface temperature gradient at the external surface increases to -1.8×10^6 after 0.2 s, but at the same time substrate surface temperature gradient decreases to -3×10^4 K·m^{-1}.

The ZrO_2 surface temperature gradient decreases in time, meanwhile temperature gradient near the ZrO_2 – underlaying material interface increases so that the maximum value of temperature gradient moves from the ZrO_2 surface to the ZrO_2 – underlaying material interface.

The substrate surface temperature gradient reaches the value -7.5×10^4 K·m^{-1} after 1 s in the case of 1 mm thick ZrO_2 and 3–10% porosity. With the increase of ZrO_2 thickness to 2 mm, substrate surface temperature gradient reaches the value -1.1×10^4 K·m^{-1} after 1 s. Increasing the ZrO_2 porosity, substrate surface temperature gradient decreases. The presence of Nimonic 90 causes further decrease of temperature gradient on the substrate surface.

5.3. Influence of TB parameters on the substrate surface heat flux

At the open substrate surface, heat flux reaches the value of 1.3×10^7 W·m^{-2} after 0.2 s and after 1 s it decreases to 5.6×10^6 W·m^{-2}.

With ZrO_2, maximum heat flux values moves in time from the ZrO_2 surface to its interface with the underlaying material. It is the similar behaviour as is observed for the temperature gradient.

With ZrO_2 of 1 mm thickness and 3–10% porosity, the maximum value of heat flux at the substrate surface 1.3×10^6 W·m^{-2} is reached after 1 s. Then, the heat flux is slowly decreasing in time. With the increase of ZrO_2 thickness to 2 mm, substrate surface heat flux has a maximum value 6.5×10^5 W·m^{-2} after 4 s. In the case of ZrO_2 of 1 mm thickness, increasing the porosity to 16–20%, the substrate surface heat flux reaches the maximum value 9×10^5 W·m^{-2} after 4 s. In the presence of Nimonic 90, heat flux increases in the bond coat area, but decreases at the substrate surface. With two-layer TB (ZrO_2 of 1 mm thickness and 3–10% porosity, Nimonic 90 of 1 mm

thickness), the Nimonic 90 surface heat flux reaches the maximum value 1.5×10^6 W·m^{-2} after 1 s, the maximum substrate surface value is 1.2×10^6 W·m^{-2} after 4 s.

5.4. Influence of TB parameters on the substrate surface normal stress

The analysis of thermally induced stresses parallel to the TB surface also elucidates the role of TB. All the surface normal stresses are compressive. Without the TB, the substrate surface normal stress reaches constant extremely high value -2.9×10^3 MPa. With ZrO_2 of 1 mm thickness and 3–10% porosity, the TB surface normal stress decreases to -8×10^2 MPa. The substrate surface normal stress gets -4.7×10^2 MPa after 1 s. With the increase of ZrO_2 thickness to 2 mm, its surface value decreases to the -9×10^1 MPa after 1 s. The increase of porosity of 1 mm ZrO_2 layer to 16–20% causes that the substrate surface normal stress reaches the value -2.8×10^2 MPa after 1 s. Nimonic 90 slows down the increase of the stress at the substrate. With the two-layer TB (ZrO_2 of 1 mm thickness and 3–10% porosity, Nimonic 90 of 1 mm thickness), the substrate surface normal stress reaches -3×10^2 MPa after 1 s. The value of thermally induced stress has overcome stability limit of used materials because of only thermoelastic problem has been solved.

The changes of the normal stress σ_{xx} along the distance from the surface of the two-layer TB are shown in Fig. 3. One can clearly observe how the Nimonic 90 surface and the substrate surface compressive stresses increase as they overcome the TB surface stress.

The influence of the TB structure on time changes of the maximum stresses in the TB and substrate is shown in Fig. 4. The TB surface normal stresses are nearly time independent, except for the beginning of the thermal shock. Constant values of normal stress indicate that neither Nimonic 90 nor substrate surface values do overcome the TB surface value. With Nimonic 90, the increase of maximum value of normal stress within the Nimonic 90 and substrate is slowed and moved to longer times. Nimonic 90 surface stress overcomes the TB surface stress at approximatly 4.2 s, substrate surface stress overcomes the TB and Nimonic 90 surface stresses somewhere between 4 and 10 s. The increase of substrate normal stress is considerably slower than in the TB without Nimonic 90.

Figure 5 shows the influence of ZrO_2 thicknesses on the maximum stresses in the structure ZrO_2-substrate. For the TB of 0.5 mm thick ZrO_2, the substrate surface normal stress exceeds the TB surface value at 0.8 s. With the increase of ZrO_2 thickness to 1 mm, this time point moves to 3 s. The increase of ZrO_2 thickness to 2 or 4 mm moves this time point behind the 10 s.

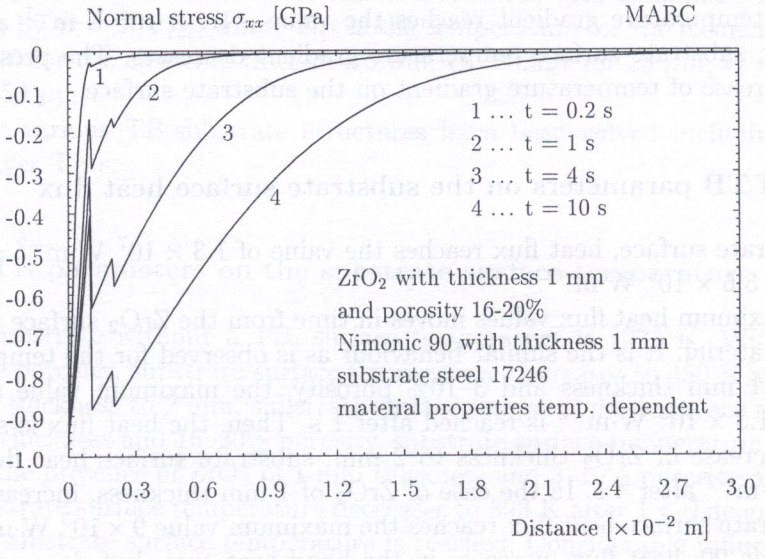

Fig. 3. Normal stress dependence on the distance from the surface

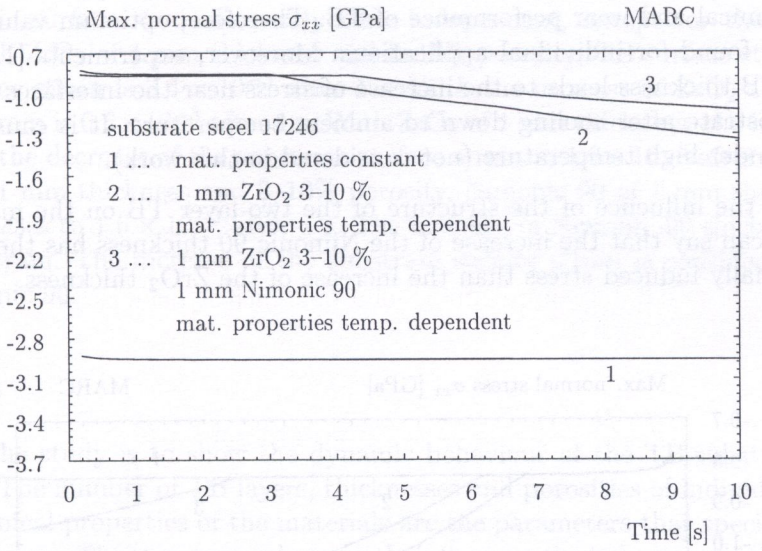

Fig. 4. Maximum normal stress time dependence – TB's usage

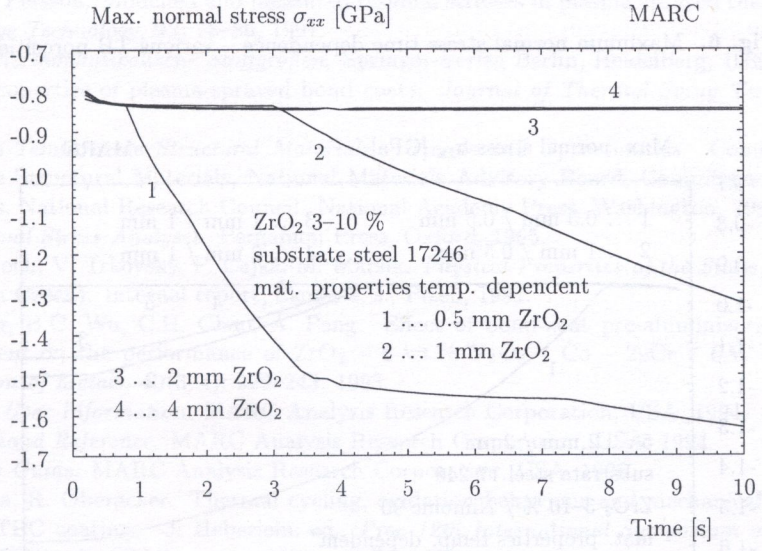

Fig. 5. Maximum normal stress time dependence – various TB thicknesses

Figure 6 shows the influence of ZrO_2 porosities on the maximum stresses in the structure ZrO_2-substrate. With the increase of ZrO_2 porosity, the increase of the substrate surface stress is slowed. We can say that the higher thickness and porosity of ZrO_2, the lower stresses will be thermally induced. However, increasing the thickness and porosity of ZrO_2 has the opposite effect – the decrease of mechanical, chemical and wear performance of TB. Therefore, optimum values of thickness and porosity has to be found for individual applications. Moreover, experiments [1, 11] show that the large increase of TB thickness leads to the increase of stress near the interfaces between individual TB layers and substrate after cooling down to ambient temperature. It is caused by the effect of stress relaxation under high temperature (not considered in this work).

Figure 7 shows the influence of the structure of the two-layer TB on the maximum stresses in the structure. We can say that the increase of the Nimonic 90 thickness has the significantly lower effect on the thermally induced stress than the increase of the ZrO_2 thickness.

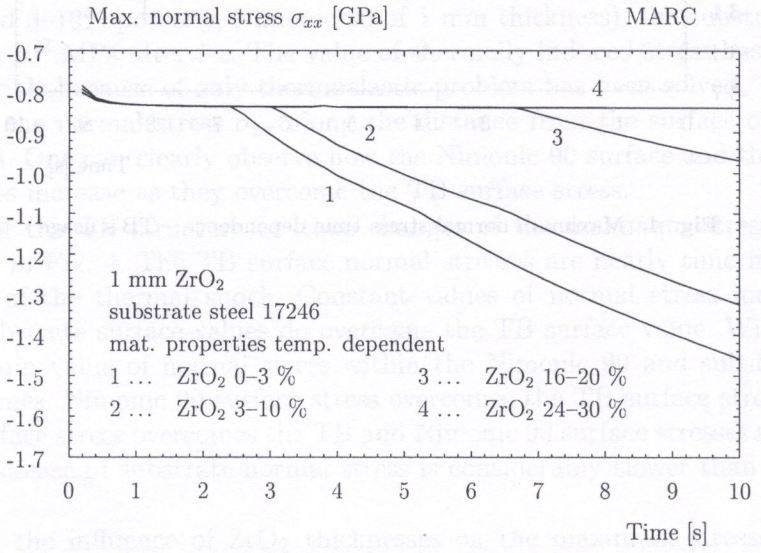

Fig. 6. Maximum normal stress time dependence – various TB porosities

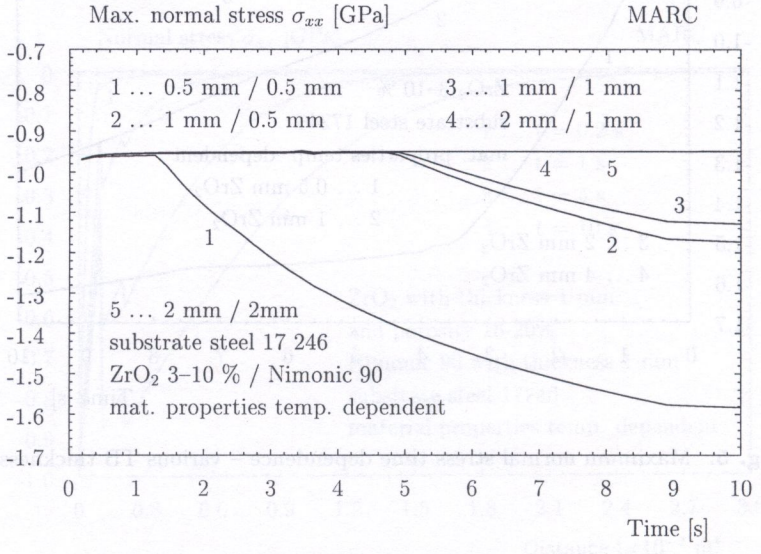

Fig. 7. Maximum normal stress time dependence – two-layer TB's

5.5. Influence of TB parameters on the substrate surface strain

Differences in thermally induced strains of each individual TB layer and of the substrate often lead to the spallation of TB. In the case of the substrate without TB, the substrate surface strain is 2.29×10^{-2}. This surface strain is nearly time independent, except for the beginning of the thermal shock. With ZrO_2 of 1 mm thickness and 3–10% porosity, TB surface strain is 8.8×10^{-3}, but substrate surface strain is 3.4×10^{-3} after 1 s. With the increase of ZrO_2 thickness to 2 mm, substrate surface strain is 0.6×10^{-3} after 1 s. With ZrO_2 of 1 mm thickness, the increase of porosity to 16–20% leads to the decrease of the substrate surface strain to 1.9×10^{-3} after 1 s. With the two-layer TB (ZrO_2 of 1 mm thickness and 3–10% porosity, Nimonic 90 of 1 mm thickness), substrate surface strain decreases to 1.6×10^{-3} after 1 s. The increase of Nimonic 90 thickness decreases the substrate surface strain. The increase of the substrate surface strain is considerably slowed down by the use of Nimonic 90.

6. Conclusions

The main task of the study is to show the dynamic behaviour of the TB-substrate system under the thermal shock. The number of TB layers, thicknesses and porosities of individual TB layers and thermal and mechanical properties of the materials are the parameters that specify the structure of the TB-substrate system. The structure subsequently influences the behaviour of this system. Special attention has to be paid to get the accurate thermal and mechanical properties of the materials. The presented results confirm the importance of TB's as a dynamic material protection against the thermal overloading. The stress relaxation under high temperature appears as an additional significant process that has not been considered yet. Therefore, the effect of stress relaxation along with the effect of residual stresses after the TB deposition is prepared to be encountered to the future modelling of TB behaviour under the condition of thermal shock.

References

[1] P. Bengtsson, Ch. Persson. Modelled and measured residual stresses in plasma sprayed thermal barrier coatings. *Surface & Coatings Technology*, **92**: 78–86, 1997.

[2] W. Blanke, ed. *Thermophysikalische Stoffgroßen*, Springer-Verlag Berlin, Heidelberg, 1989.

[3] W.J. Brindley. Properties of plasma-sprayed bond coats. *Journal of Thermal Spray Technology*, **6**(1): 85–90, 1997.

[4] *Coatings for High-Temperature Structural Materials – Trends and Opportunities.* Comittee on Coatings for High-Temperature Structural Materials, National Materials Advisory Board, Commission on Engineering and Technical Systems, National Research Council. National Academy Press, Washington, 1996.

[5] D.J. Johns. *Thermal Stress Analyses.* Pergamon Press, Oxford, 1965.

[6] J. Kuneš, O. Vavroch, V. Trkovský, F. Čejka, M. Maršík. *Physical Properties of the Steels, Part I.: Steels of the Class 15 to 19*, (in Czech). Internal report, Škoda a. s., Plzeň, 1991.

[7] W. Lih, E. Chang, B.C. Wu, C.H. Chao, A. Peng. Effect of bond-coat pre-aluminization and pre-oxidation duplex pretreatment on the performance of ZrO_2 – 8 wt.% Y_2O_3 / Co – 29Cr – 6Al – 1Y thermal barrier coatings. *Oxidation of Metals*, **40**(3/4): 229–243, 1993.

[8] *Marc, Volume A, User Information.* MARC Analysis Research Corporation, USA, 1994.

[9] *Mentat II., Command Reference.* MARC Analysis Research Corporation, USA, 1994.

[10] *Mentat II., User's Guide.* MARC Analysis Research Corporation, USA, 1996.

[11] J. Musil, M. Alaya, R. Oberacker. Thermal cycling, oxidation behaviour and mechanical properties of graded and duplex PSZ TBC coatings. J. Heberlein, ed., *Proc 12th International Symposium on Plasma Chemistry*, Vol. **II**, 915–920. University of Minnesota, Minneapolis, 1995.

[12] B.E. Neimark. *Fizicheskie Svoistva Stalei i Splavov, Primeniaemych v Energetike.* Energiia, Moscow, 1967.

[13] N.A. Puchkelevich, E.Ia. Litovskii. *Teplofizicheskie Svoistva Ogneuporov.* Metallurgiia, Moscow, 1982.

[14] Kh.G. Schmitt-Thomas, U. Dietl. Thermal barrier coatings with improved oxidation resistance. *Surface and Coatings Technology*, **68/69**: 113–115, 1994.

[15] T.E. Strangman. Thermal strain-tolerant abradable thermal barrier coatings. *Journal of Engineering for Gas Turbines and Power*, **114**: 264–267, 1992.

[16] J.H. Sun, E. Chang, C.H. Chao, M.J. Cheng, The spalling modes and degradation mechanism of ZrO_2 – 8 wt.% Y_2O_3 / CVD – Al_2O_3 / Ni – 22Cr – 10Al – 1Y thermal barrier coatings. *Oxidation of Metals*, **40**(5/6): 465–481, 1993.

[17] Y.S. Touloukian, C.Y. Ho, eds. *Thermophysical Properties of Matter — The TPRC Data Series.* IFI/Plenum, New York, 1970.

[18] H.L. Tsai, P.C. Tsai. Performance of laser-glazed plasma-sprayed (ZrO_2 – 12 wt. % Y_2O_3)/(Ni – 22 wt. % Cr – 10 wt. % Al – 1 wt. % Y) thermal barrier coatings in cyclic oxidation tests. *Surface and Coatings Technology*, **71**: 53–59, 1995.

[19] O.C. Zienkiewicz. *The Finite Element Method.* McGraw-Hill, New York, 1973.